POROUS MEDIA VISUALIZATION AND CHARECTERIZATION VIA MATHEMATICAL MORPHOLOGY

B.S. DAYA SAGAR

http://www.isibang.ac.in/~bsdsagar

Systems Science and Informatics Unit (SSIU)

Indian Statistical Institute-Bangalore Centre

2D Topological Pore Characterization

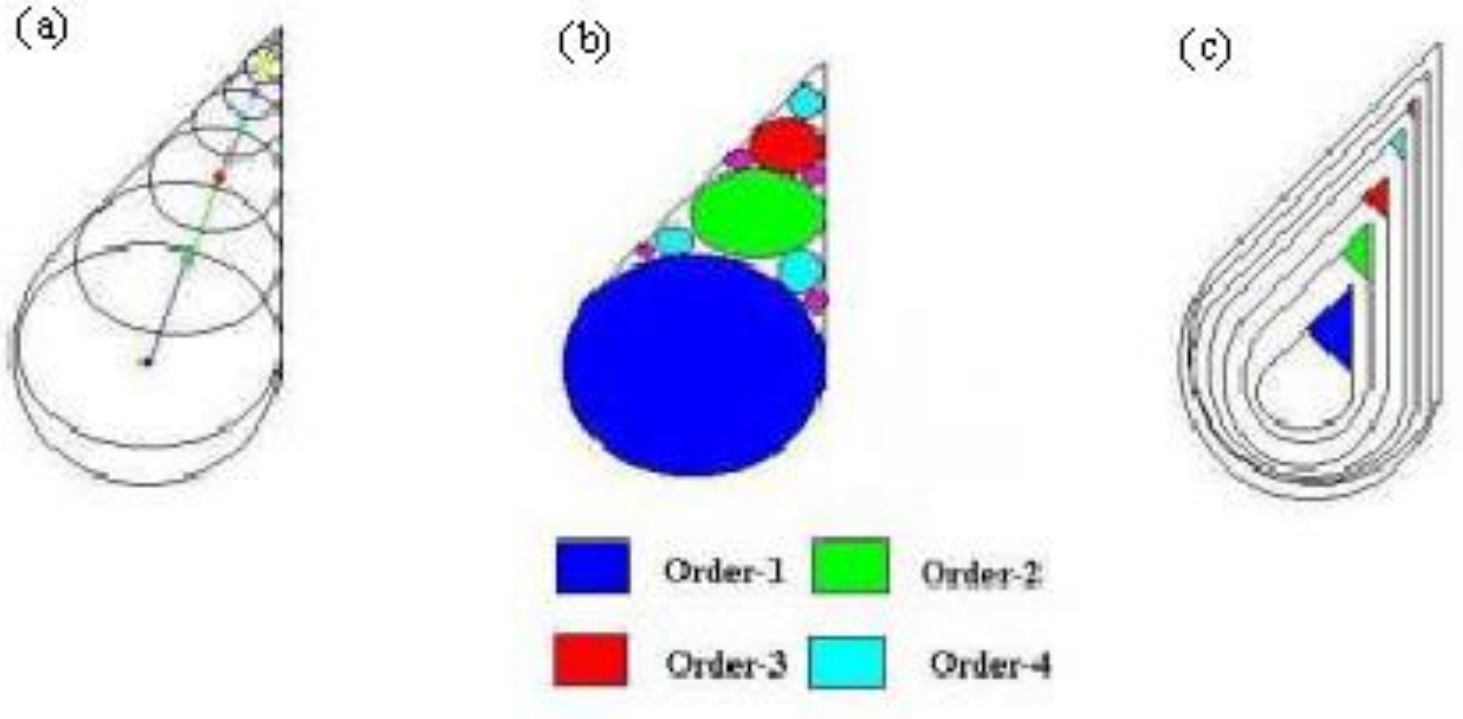

Figure1: The models of (a) pore connectivity network (channel), (b) pore body and (c) pore throat

Thin section (macro-level)

Rock sample

Image Acquisition (micro-photograph)

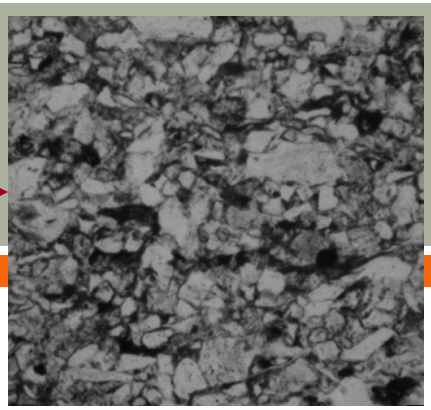

Digital image

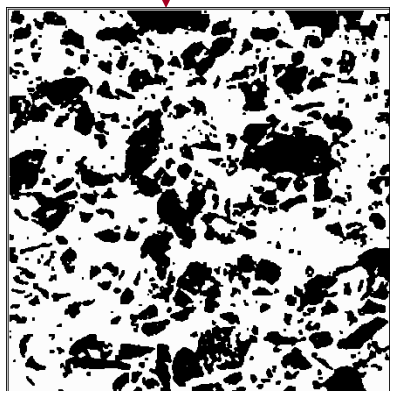

2D topological characterization (binary image)

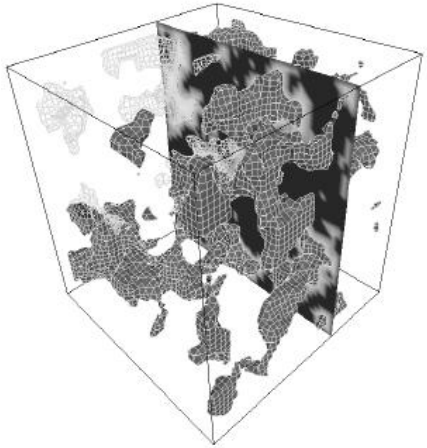

3D reconstruction of pore structure (micro level)

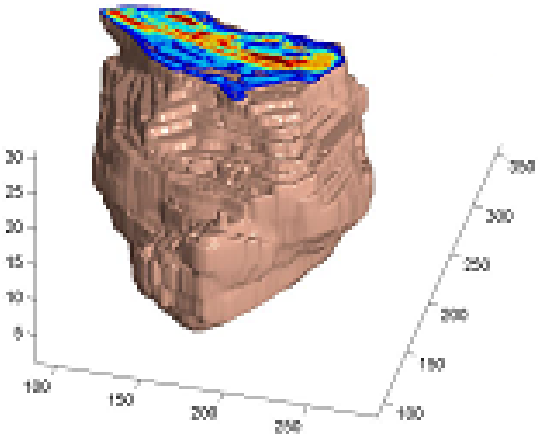

3D reconstruction of rock sample (macro level)

Figure 2: The diagram show the macro and micro levels analysis on rock sample

Methodology

- Study on mathematical morphology techniques
- By using the mathematical morphology techniques, we work on
  - 2D Topological Analysis
    1. Morphological decomposition techniques
    2. Pore connectivity network techniques
    3. Pore throat techniques
    4. Reconstruction by overlapping and non-overlapping techniques
  - and 3D Topological Analysis

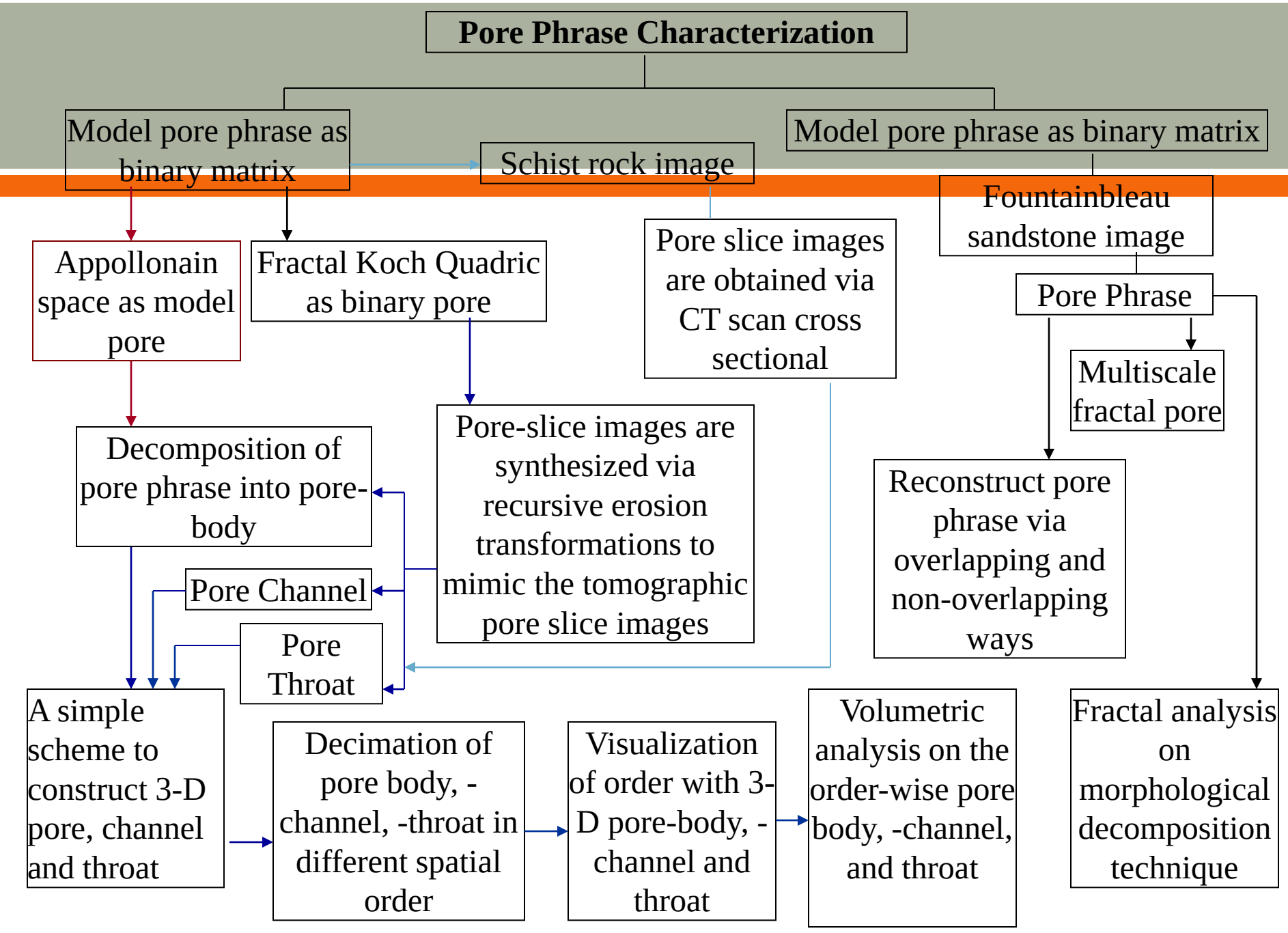
Pore Phrase Characterization
Model pore phrase as binary matrix
Schist rock image
Model pore phrase as binary matrix
Appollonain space as model pore
Fractal Koch Quadric as binary pore
Pore slice images are obtained via CT scan cross sectional
Fountainbleau sandstone image
Pore Phrase
Multiscale fractal pore
Decomposition of pore phrase into pore-body
Pore-slice images are synthesized via recursive erosion transformations to mimic the tomographic pore slice images
Reconstruct pore phrase via overlapping and non-overlapping ways
Pore Channel
Pore Throat
A simple scheme to construct 3-D pore, channel and throat
Decimation of pore body, -channel, -throat in different spatial order
Visualization of order with 3-D pore-body, -channel and throat
Volumetric analysis on the order-wise pore body, -channel, and throat
Fractal analysis on morphological decomposition technique

Procedures of Morphological Decomposition

- We considered the decomposition procedure that utilizes non-overlapping structuring elements with sizes distributed randomly from radius R_{max} to R_{min} in *pore* image.
  - The available *pore* space is decomposed with the structuring elements of the higher radius (R_{max}).
  - Once filling the decomposed R_{max} , it is followed by the procedure that reduces the radius of the structure elements.
  - The procedure is repeated until leftover pore is filled with the structuring element of the pore with minimum radius (R_{min}).

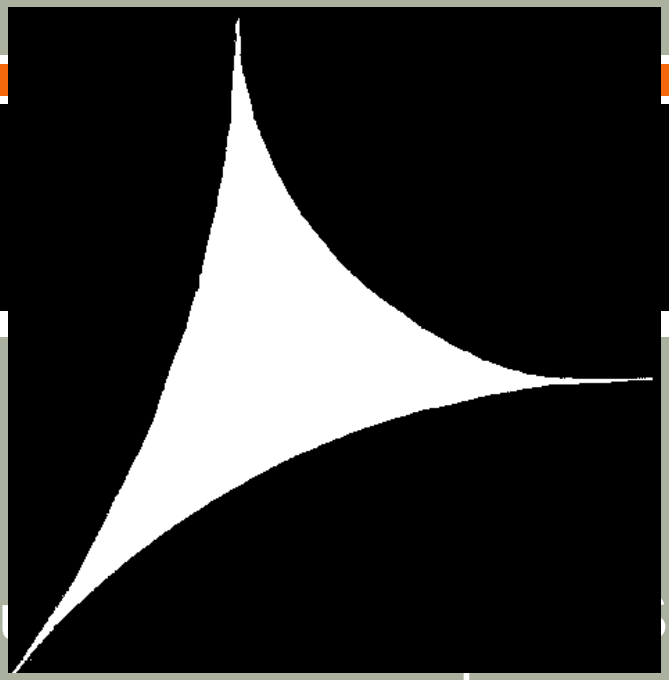

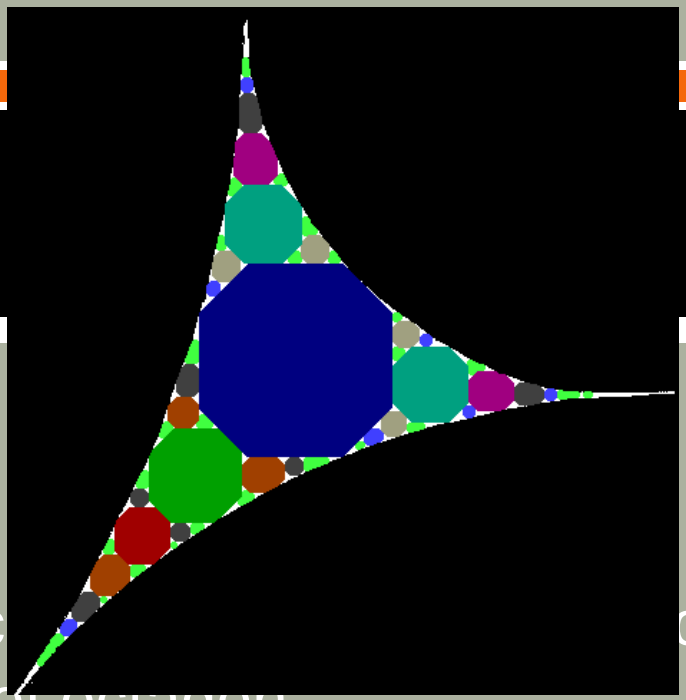

Figu pac osition by means of octagon.

To estimate fractal dimension

- This type of decomposition facilitates a procedure to estimate the dimension, akin to fractal dimension, through a power-law relationship which can be represented by

$$N(r) \propto r^{-\alpha} \qquad \text{with} \quad D = \alpha - 1 \qquad (2)$$

where N - the number of decomposed shapes,

r - radius,

α - slope of the regression line,

D - fractal dimension.

This procedure includes systematic use of multiscale *opening* and simple logical operators. The following set of eqns shows how to decompose a shape following these morphological transformations.

$$M_2 = M_1 \setminus M_1 \circ S_n$$
$$M_3 = M_2 \setminus M_2 \circ S_n$$
$$M_n = M_{n-1} \setminus M_{n-1} \circ S_n \quad \text{and} \quad M_{n+1} = M_n \setminus M_n \circ S_n$$
$$M_n = M \quad \text{and} \quad M_{n+1} = \phi$$
$$M_{\text{Decomp}} = (M \circ S_n) \cup (M_1 \circ S_n) \cup (M_2 \circ S_n) \cup \ldots \cup (M_{n-1} \circ S_n) \quad (3)$$

$$M_n \subset M_{n-1} \subset \ldots \subset M_3 \subset M_2 \subset M_1 \subset M$$

where M is digital binary pore.

- A discrete binary pore image, *M* (Fig. 8b), is defined as a values between 0 and 1.

- Each structuring template (*S*) has a designed shape that acts as a probe. For examples, structuring elements of rhombus, square, octagon.

- A morphological operation transforms *M* to a new image by a structuring element *S* to obtain decomposed shape.

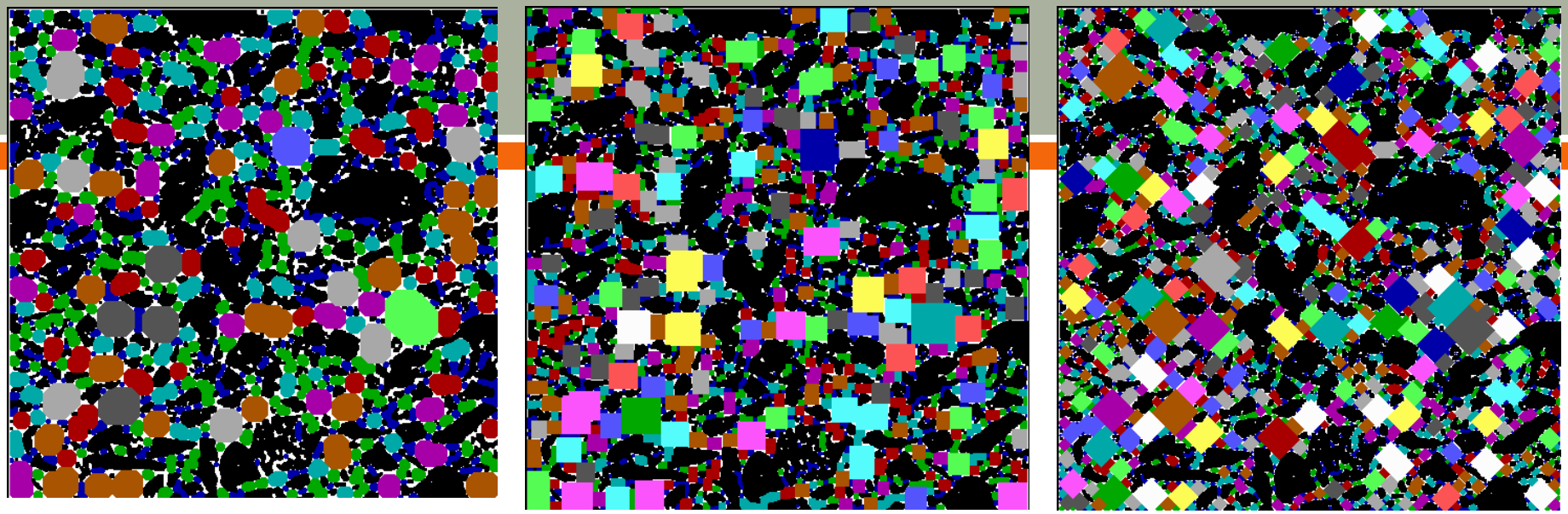

(a) (b) (c)

Figure 9 (a-c): Decomposition of pore by means of octagon, square and rhombus

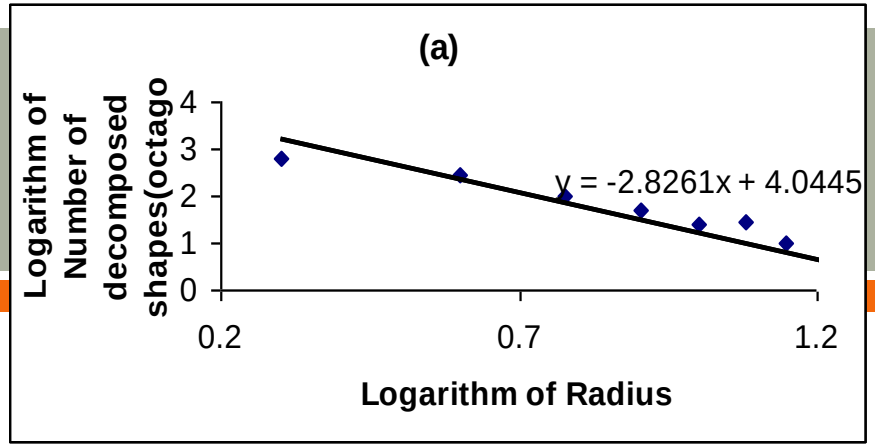

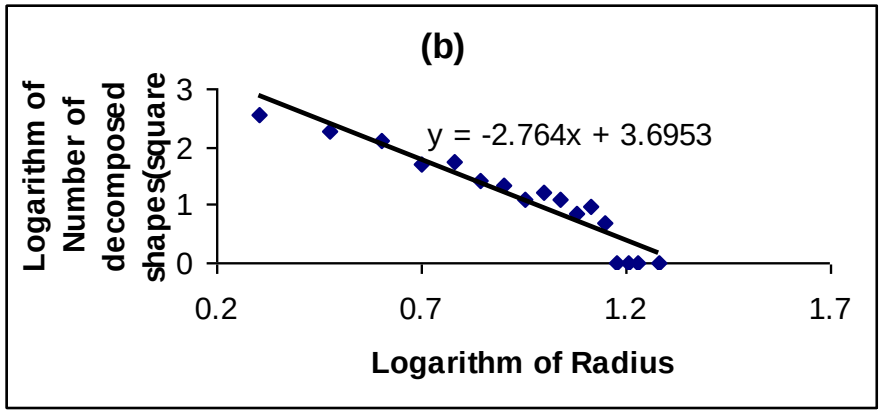

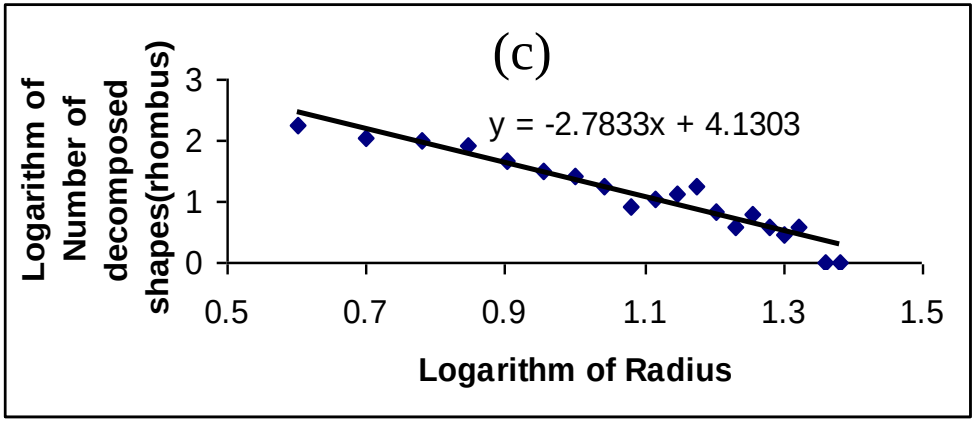

Figure 10(a - c): Graphical plots of logarithm of number of decomposed shapes versus logarithm of radius of structuring element for octagon, square and rhombus.

Table 1: The estimation of Fractal dimension

Closing at pore space	Fractal Dimension (D)		
	Rhombus	Square 3x3	Octagon
Morphological decomposition	1.7833	1.764	1.8261

Summary of morphological decomposition

- The smaller the size of primary pattern e.g. square, rhombus that is used to decompose the pore-space, the larger the, number of cycles or, radius is required for decomposition.
- The fractal dimensions of this decomposition pore-space, derived by means of the number-radius relationship by these three types of structuring elements are 1.8, 1.76, and 1.78.
- From the power law of relationship ($N(r) \propto r^{-\alpha}$), the number of cycles or, radius is required to decompose depend on the radius of structuring template (rhombus and square - $n+1$, octagon - $n+2$).

3. Fractal Analysis of Pore Connectivity Network

(Teo Lay Lian, IEEE Proceedings of the 3rd International Symposium on Image and Signal Processing and Analysis, (2003) v. 2, p.686 – 689)

Part I: Fractal Analysis of pore connectivity network

- The **pore connectivity networks** (***PCNs***) are extracted from pore space of sandstone microphotograph.

(Pore connectivity network is the skeleton in pore media)

- These networks are derived by considering structuring templates such as ***octagon, square*** and ***rhombus***. The fractal dimensions are estimated for these loop-like *PCNs*.

- From the number-size relationship, the fractal dimensions of pore-space estimated, by considering these structuring elements, yield the values of **1.67, 1.68** and **1.69** arising in our proposed methodology of morphological decomposition.

- These transformations can be visualized as working with two pore images namely the image being processed (M), and a structuring template (S).

- applied fractal-skeletal based channel network (*F-SCN*) model (Sagar et. al, 2001) to extract the pore connectivity network.

Examples (rhombus as a probe):

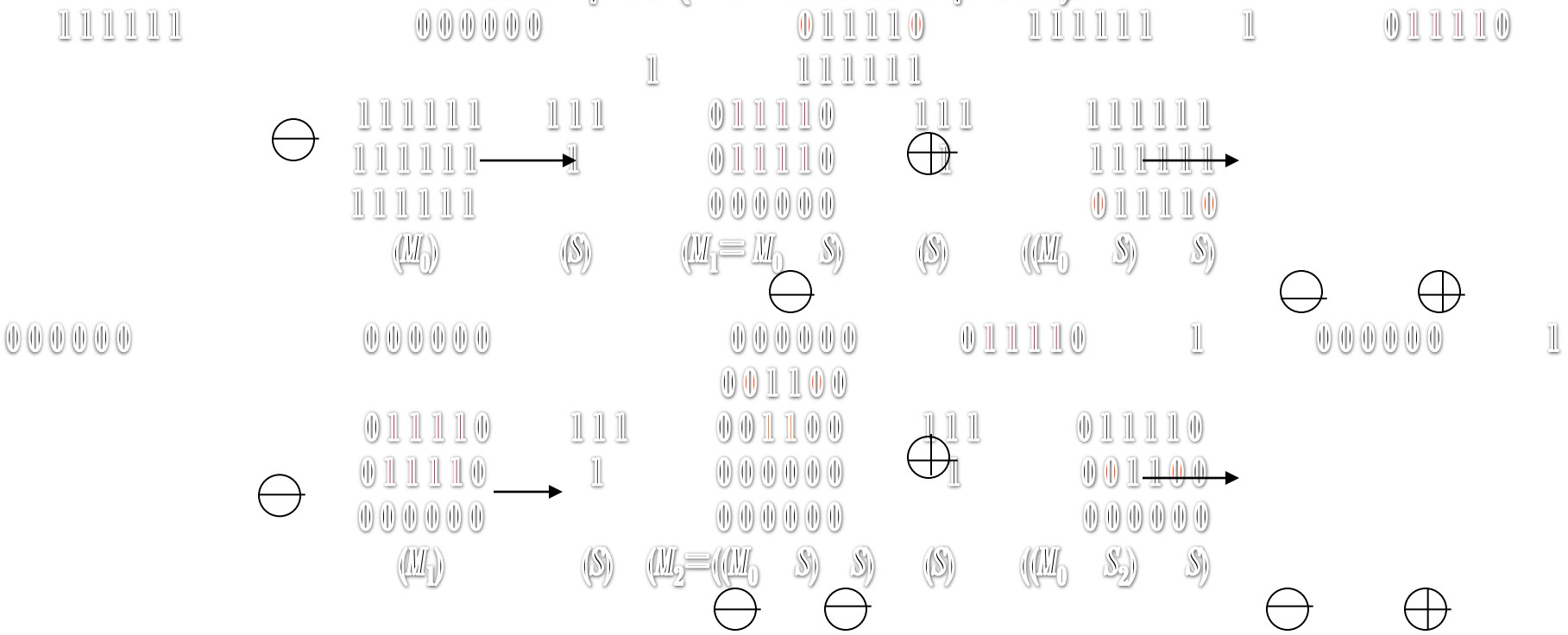

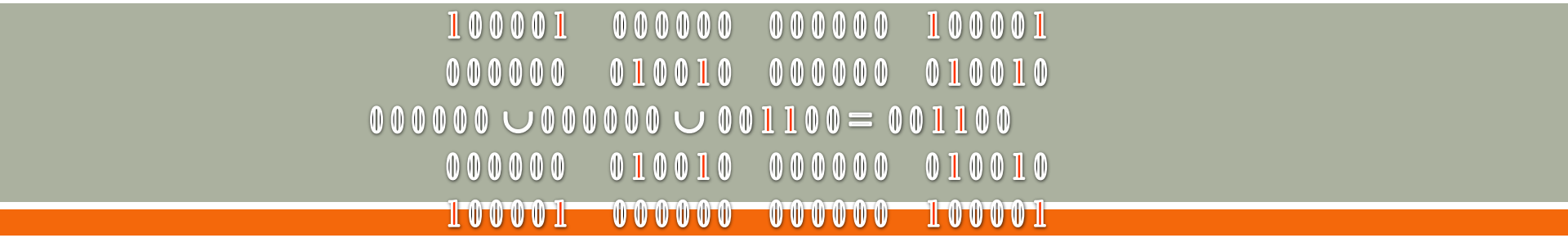

The model which forming pore connectivity is similar to channel network.

This network, *PCN* (*M*), can be defined mathematically as

$$PCN_n(M) = (M \ominus S) \setminus \{[(M \ominus S_n) \ominus S] \oplus S\} \qquad (4a)$$

$$PCN(M) = \bigcup_{n=0}^{N} PCN_n(M) \qquad n = 1, 2, \ldots, N \qquad (4b)$$

- where $PCN_n(M)$ denotes the *n*th channel subset of fractal basin (M).

- We are using structuring elements such as rhombus, square and octagon to extract pore connectivity network from pore-space of sandstone image.

- To estimate the fractal dimension,

The power law relationship can be represented by

$$N(r) \propto r^{-\alpha} \quad \text{with} \quad D = \alpha \qquad (5)$$

where N, r, α, and D respectively represent the number of pixels of pore connectivity network, size of structuring elements, slope of the regression line, and fractal dimension.

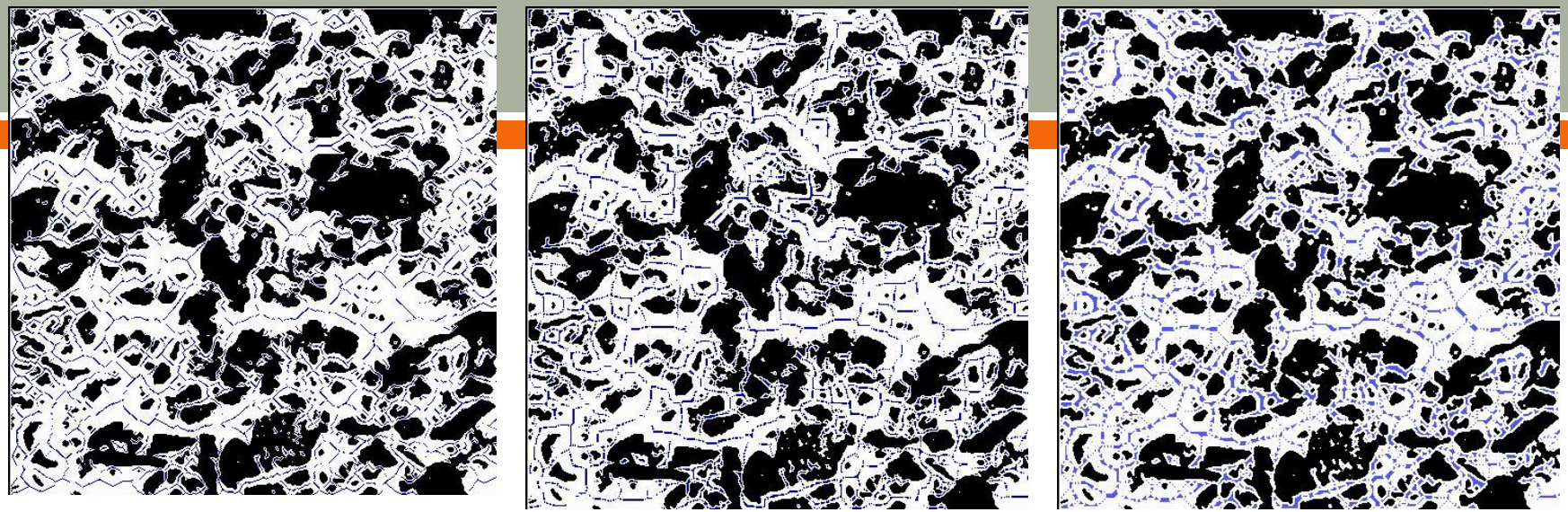

(a) (b) (c)

Figure 11: The extraction of pore connectivity network of structuring elements:

(a) rhombus,

(b) square and

(c) octagon.

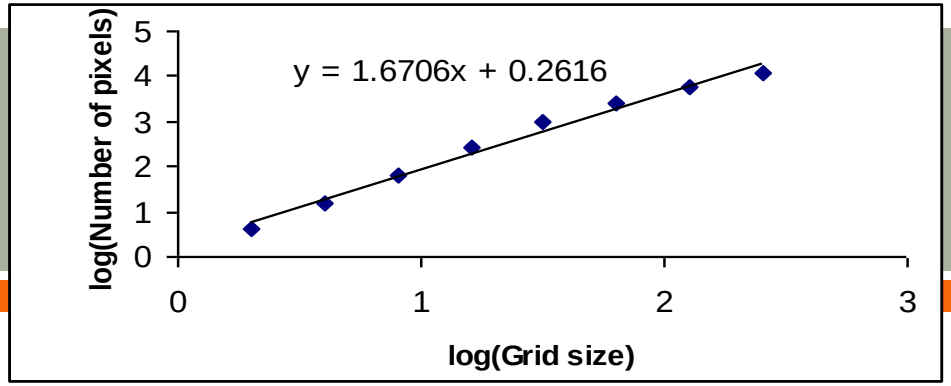

(a)

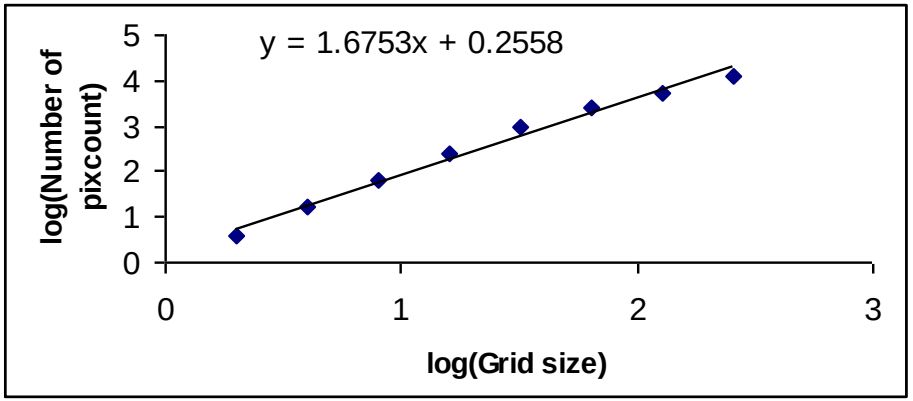

(b)

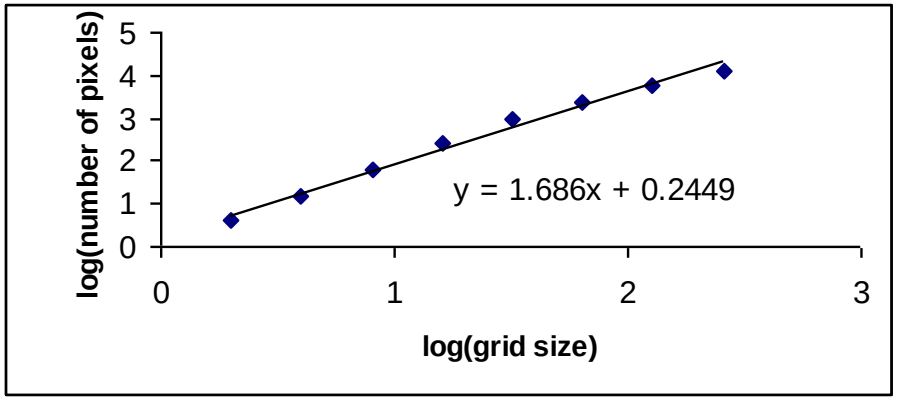

(c)

Figure 12(a-c): Graphical plots between of number of pixels of pore connectivity network versus size of structuring element for (a) rhombus, (b) square and (c) octagon.

The methods of morphological decomposition and pore connectivity network

- We calculate the fractal dimension through our proposed morphological decomposition technique, however, we also estimate the fractal dimension of pore connectivity through the existing technique, i.e. box counting method

- The results of fractal dimension shown that these two procedures of morphological decomposition and pore connectivity network are similar.

Part II: Further studies on multi-scale pore connectivity network

- Analyze the relationships between fractal dimension and the multi-scale dimension of pore connectivity networks (PCNs) in this pore media.

- Investigate the different dimensions of pore space with applying opening transformations to obtain the multi-scale dimensions of pore space. Furthermore, we apply the mathematical morphology technique to obtain the pore connectivity network.

- The lengths of pore connectivity appear in the branching network forms that are irregular and fragmented in sizes. As a result, we estimate fractal dimension (D) with box counting method

Examples of multiscale pore connectivity network with structuring element of square

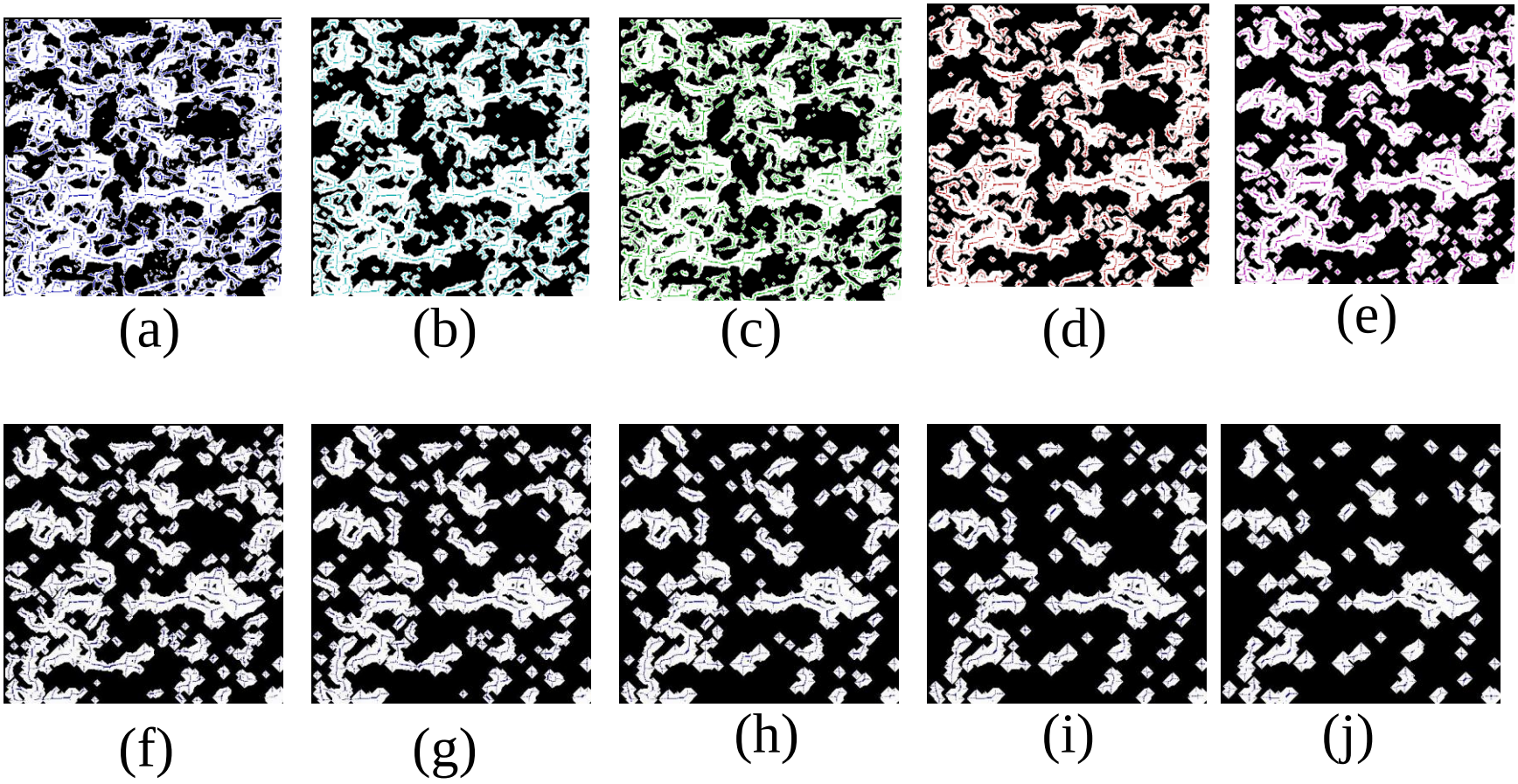

Figure 13(a-j): The extraction of pore connectivity network by square structuring element at multiscale dimensions of pore space

Summary of the multiscale dimension of pore connectivity network

- Less intricacy of connectivity networks is observed in higher opening cycles of model images due to the fact that decreasing of the area of small particles at pore space

- From the results of fractal dimension in Figure 14, it is shown that the values of fractal dimension of the pore connectivity network for rhombus, square and octagon is decreasing (scaling) as the opening process increasing

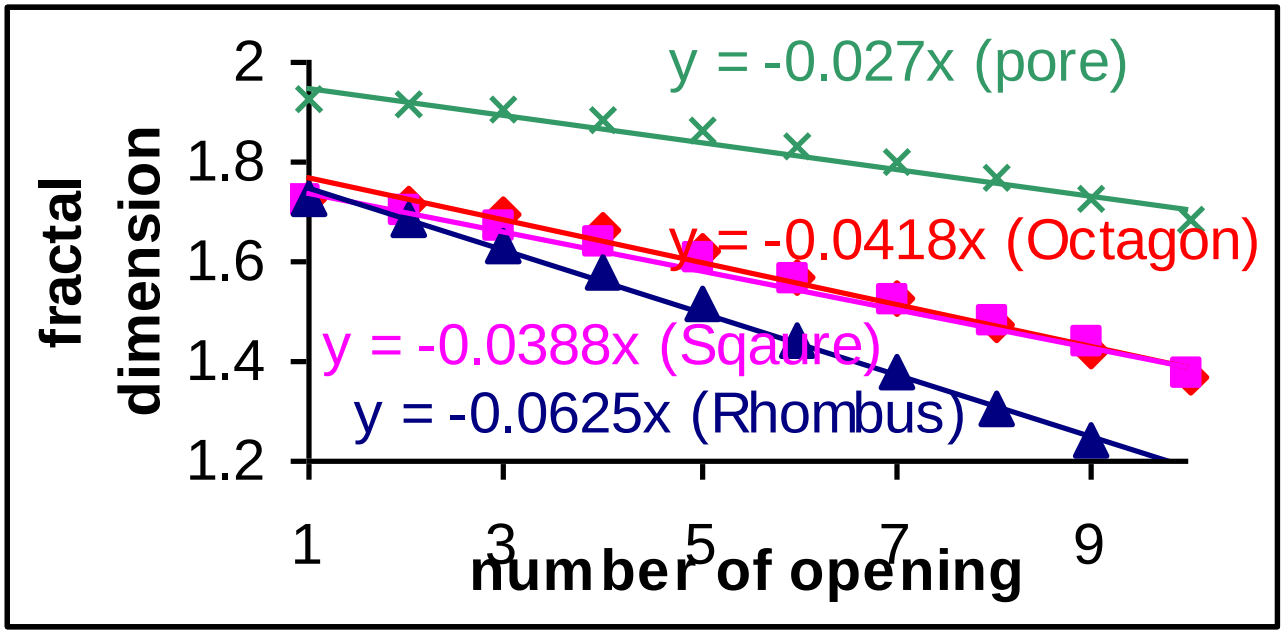

Figure 14:The relationship of fractal dimension with the number of opening process

4. Comparison of Reconstruction Techniques

(Teo Lay Lian, B.S. Daya Sagar, Journal of Microscopy (Oxford), v. 219, Pt 2, p. 76-85, 2005)

Random pore space reconstruction

- The random pore space is reconstructed in two ways from minimum morphological information through:
  (a) overlapping and
  (b) non-overlapping disks of various shapes and sizes

- The employed structuring elements to carry out this analysis include the octagon, the square and the rhombus

Overlapping reconstruction

- Overlapping reconstruction is reconstructed by selectively dilating these connectivity network points with three structuring templates as shown mathematically below

$$D\text{-}PCN_n(M) = PCN_n(M) \oplus S_n \,, \quad n = 1, 2, \ldots, N \qquad (6a)$$

- Dilated portions thus achieved are combined and formed the overlapping reconstructed pore image

$$RECON(O) = \bigcup_{n=1}^{N} \left[PCN_n(M) \oplus S_n \right] \qquad (6b)$$

Non-overlapping reconstruction

- The non-overlapping procedure (morphological decomposition) is decomposed with non-overlapping structuring elements into the pore space

- To compute the efficiency of these two techniques, we find the probability cumulative distribution functions

$$\frac{A\left[RECON(M)\right]}{A\left[M\right]} = \frac{A\left[\bigcup_{n=1}^{N}\left[PCN_n(M) \oplus S_n\right]\right]}{A\left[M\right]} \qquad (7)$$

- The results achieved through two types of reconstruction of sandstone pore are compared.

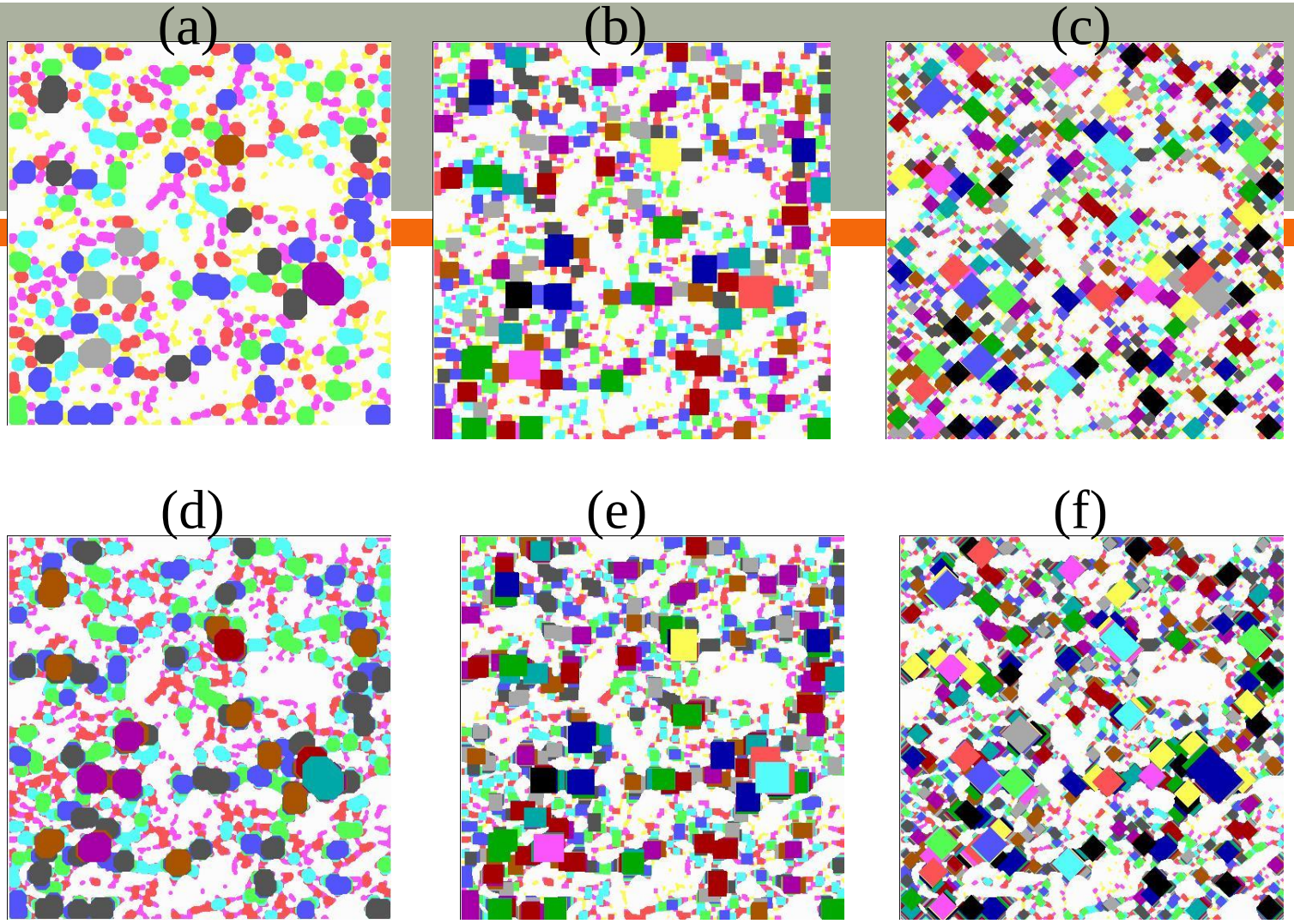

Figure 15: Colour-coded reconstructed pore images, (a-c) pore image reconstructed via non-overlapping procedure respectively by means of octagon, square, and rhombus structuring elements; and (d-f) pore image reconstructed via overlapping approach respectively by means of octagon, square, and rhombus structuring elements.

The results of probability cumulative distribution function (PCD) of overlapping and non-overlapping reconstructions

First times opening image	Ratio of area of reconstructed pore image to the original pore image		
	octagon	square 3x3	rhombus
Overlapping reconstructed image	0.9484	0.9849	0.9873
Non-Overlapping reconstructed image	0.8531	0.9315	0.9164

Table 2. Ratios of areas between original pore image and pore image reconstructed (PCD) via overlapping and non-overlapping approaches.

Summary of overlapping and non-overlapping techniques

- The pore space reconstructed via overlapping procedure matches closely to the original pore space as compared to the pore space reconstructed through the non-overlapping procedure

- However, the non-overlapping reconstruction does not provide good results in reconstruction, which is due to the fact that many regions within the original pore space are not filled

- The overlapping reconstruction is done with more accuracy with the rhombus when compared to the octagon and the square.

3D reconstruction techniques

Part I : Proposed 3D reconstruction techniques on image of triadic Koch curve

- Apply the techniques used in 2D topological to 3D modeling
  - Pore bodies
  - Pore connectivity network or channel network
  - Pore throat

- To analyze the macro-level of morphology reconstruction technique, the employed structuring element to carry out this analysis is the octagon.

Methodology in 3D reconstruction on image of triadic Koch curve

- We perform morphological erosion technique at the triadic Koch curve. We generate different slices of this model pore by iteratively eroding till it vanishes
- These recursively eroded pore spaces to different degrees are systematically considered as slices and a 3D modeling is constructed as shown in

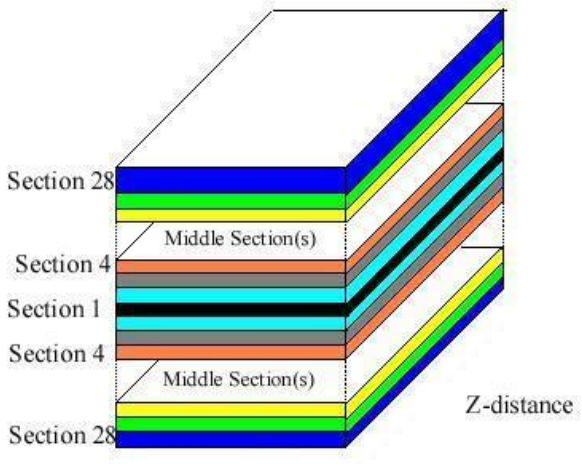

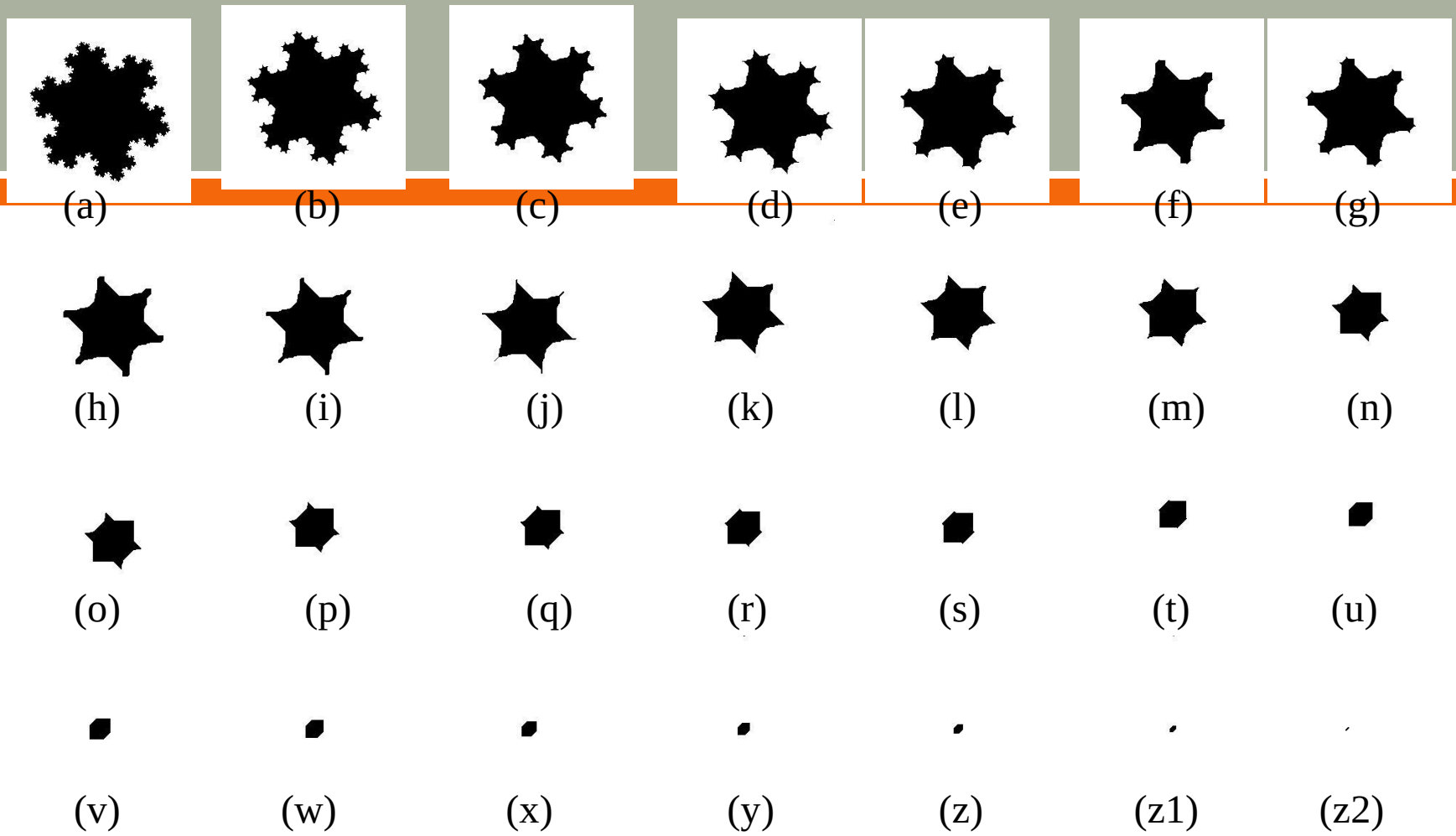

Figure 16: Image **triadic Koch curve** by applying successive morphological erosion operations with structuring element of octagon.

Analysis of 2D topological in 3D modeling

- To visualize the existing 2D topological analysis (pore bodies, pore channel and pore throat) in 3D space,
  - we consider to extract slice-wise pore channel, -throat, and –body networks from 2D pore features and reconstruct pore-connectivity, -throat, and –body network in three-dimensional space.

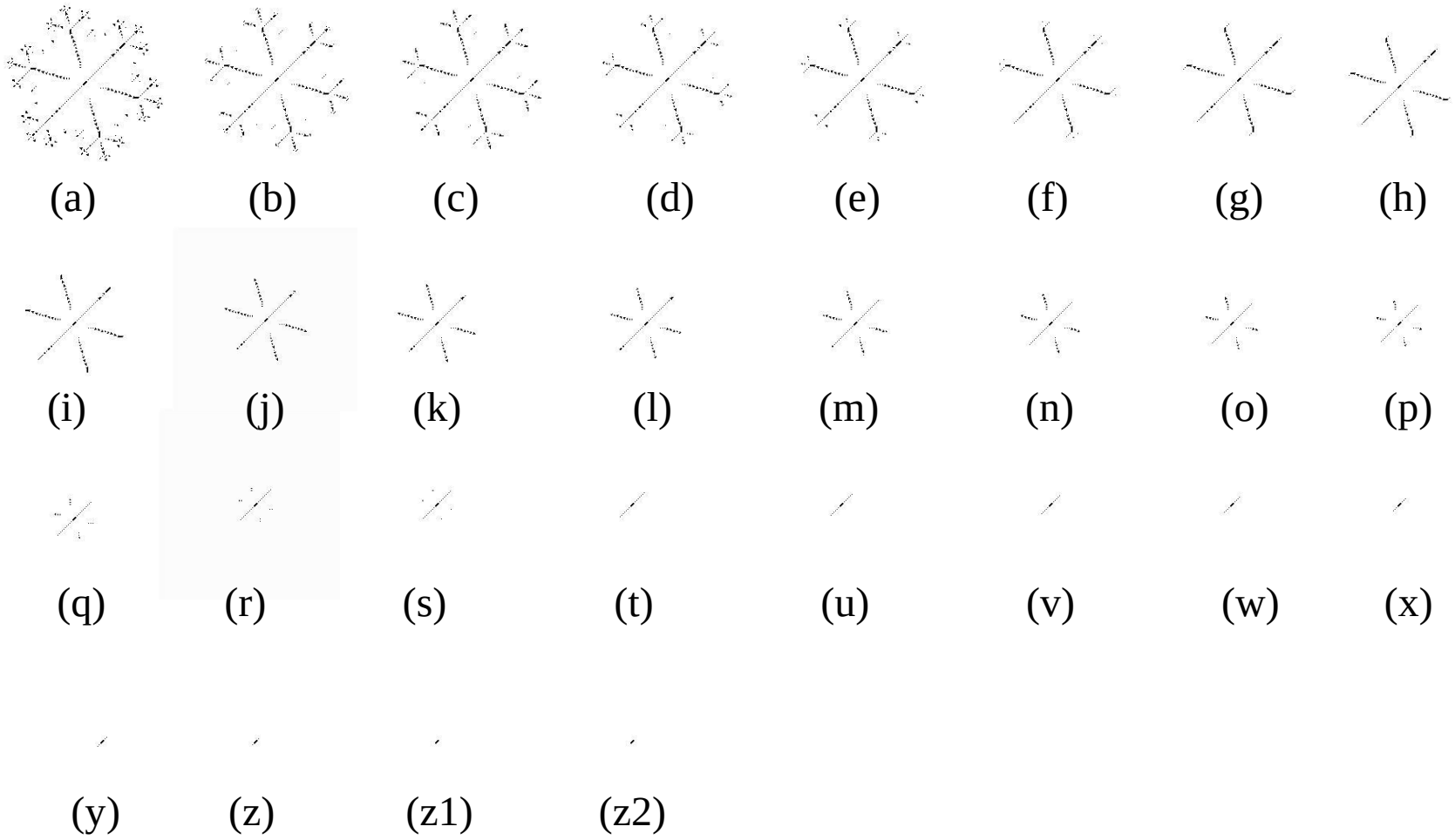

Figure17: The extracting of pore channel from eroded of **triadic Koch curve** images (Fig. 16) by structuring element of octagon.

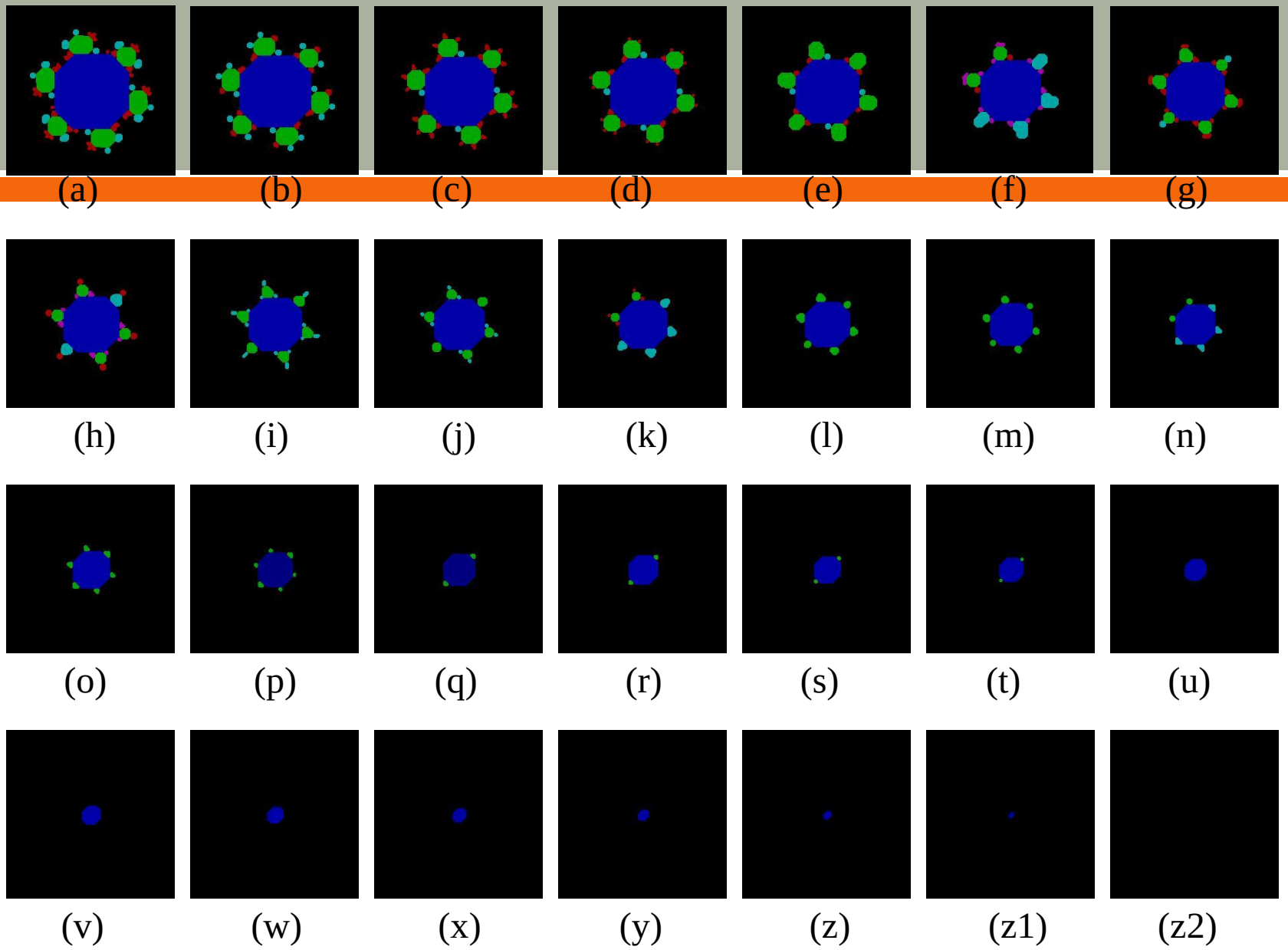

Figure 18: Extraction of pore bodies from eroded **triadic Koch curve** images (Fig. 16) by octagon structuring element.

Extraction of pore throat

- If we applied n^{th} size of structuring element to perform opening in (eqn. 4a), the resultant information would obtain n^{th} size pore-throat

(8a)

- The union of n^{th} size pore-throats would provide pore-throats of all existing sizes in the pore structure as shown in

$$PTN_n(M^j) = (M^j \ominus nS) \setminus [(M^j \ominus nS) \circ nS], n = 0,1,\ldots,N; j = 1,2,\ldots,N$$

(8b)

$$\mathrm{PTN(M)} = \bigcup_{n-0}^{N} \mathrm{PTN_n}(M)$$

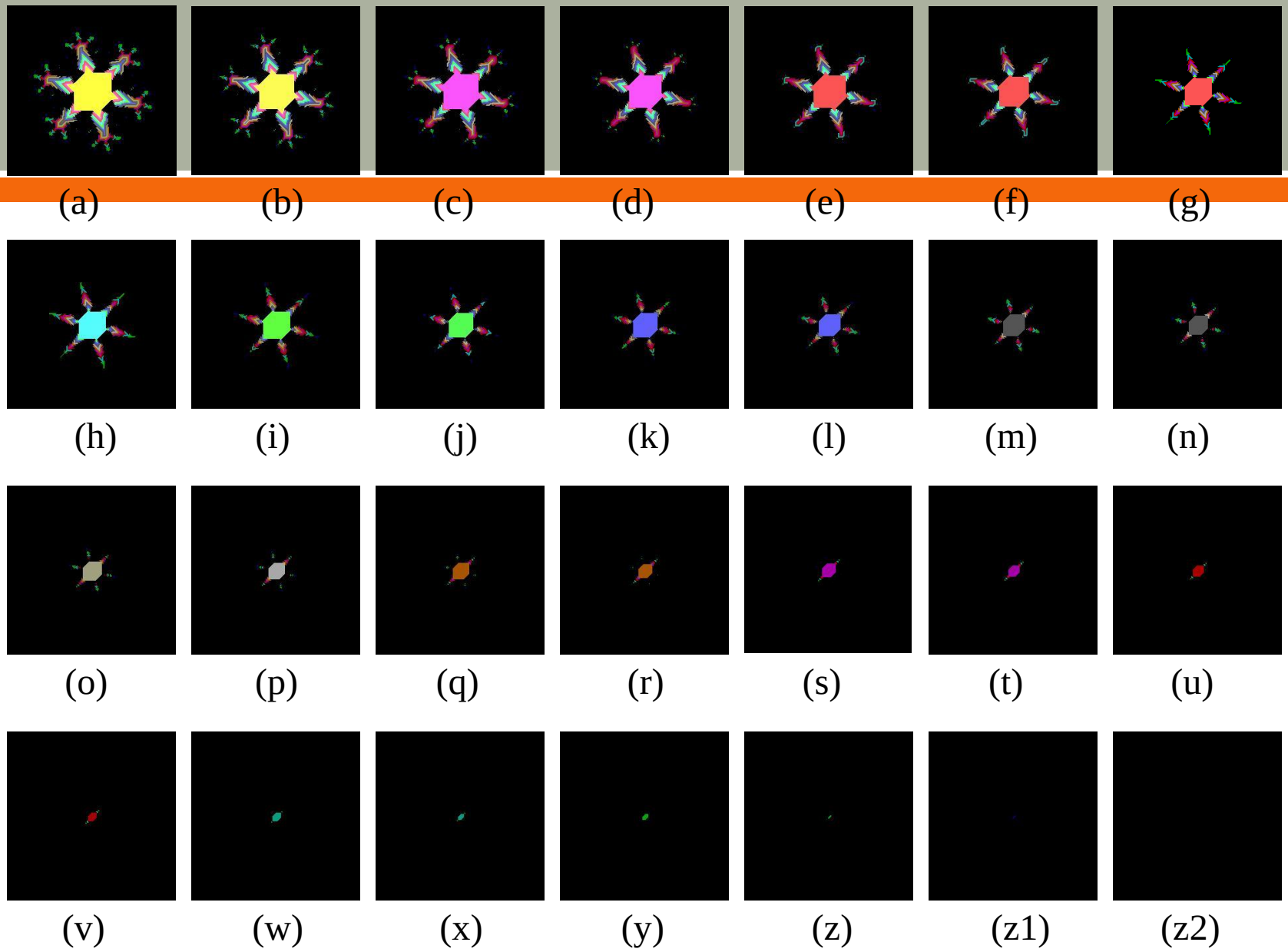

Figure 19: Extracting pore throat from eroded **triadic Koch curve** images (Fig. 16) by structuring element of octagon.

Figure 20:

Top and side views of 3D model at

(a) binary pore (Figure 16),

(b) pore-bodies (Figure 18),

(c) pore-channel (Figure 17), and

(d) pore-throat (Figure 19)

of **triadic Koch curve**

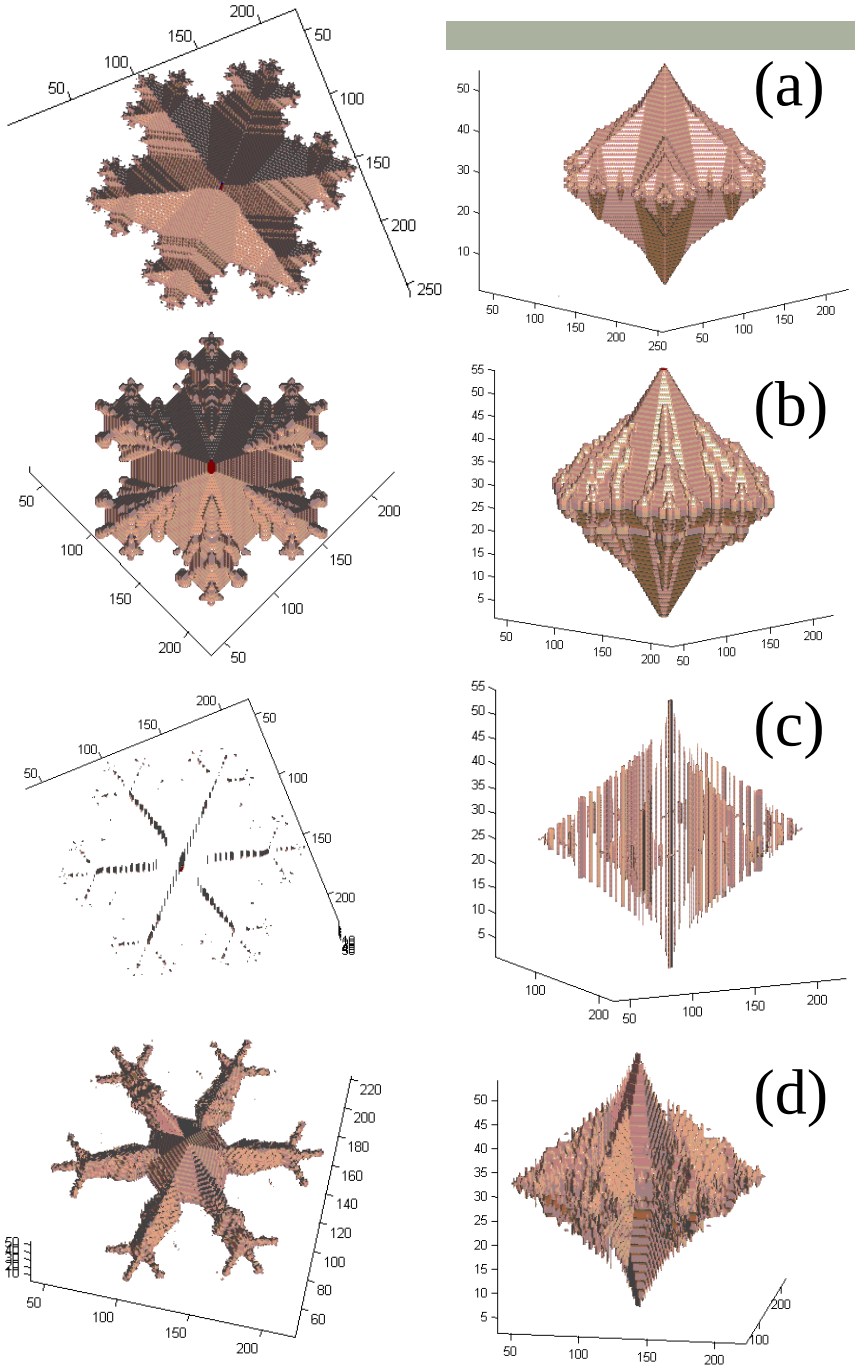

The 2D topological techniques

- The 2D topological techniques (i.e., pore channel, pore bodies, pore throat) is constructed from ranging 0 to N decomposed respectively for each pore image slice is represented by the set:

Example of pore channel:

$$PCN(G) = \left\{ \left[PCN^{1}(G) \right], \left[PCN^{2}(G) \right], \cdots, \left[PCN^{N-1}(G) \right], \left[PCN^{N}(G) \right] \right\} \quad (9a)$$

where

$$\left.\begin{aligned} PCN^{1}(G) &= \left\{ \left[PCN_{N}(M^{1}) \right], \left[PCN_{N}(M^{2}) \right], \cdots, \left[PCN_{N}(M^{N-1}) \right], \left[PCN_{N}(M^{N}) \right] \right\} \\ PCN^{2}(G) &= \left\{ \left[PCN_{N-1}(M^{1}) \right], \left[PCN_{N-1}(M^{2}) \right], \cdots, \left[PCN_{N-1}(M^{N-1}) \right], \left[PCN_{N-1}(M^{N}) \right] \right\} \\ &\vdots \\ PCN^{N}(G) &= \left\{ \left[PCN_{1}(M^{1}) \right], \left[PCN_{1}(M^{2}) \right], \cdots, \left[PCN_{1}(M^{N-1}) \right], \left[PCN_{1}(M^{N}) \right] \right\} \end{aligned}\right\} \quad (9b)$$

and j = ranging from 0 to N

Example of orders in pore body

- The number of order or subtracted portions that may appear while decomposing a pore space depends on its size and shape, as represented in following equation

$$M_{i+1}^{j} = \left[M_i^j \setminus M_i^j \circ nS \right] \qquad (10)$$

where i = 0, 1, 2,..., N; *j* =1, 2, ..., N.

$$PBN(M^j) = \bigcup_{i=0}^{N} \left(M_i^j \text{on} S \right) \qquad (11)$$

1) The orders of fragmentation can be divided into

1st order fragmented pore body

- the N^{th} level decomposed body from all the slices that put in a separate stack

2nd order fragmented pore bodies

- The decomposed pore bodies which are smaller than the N^{th} level decomposed disks from the previous order (from the reminder of respective slices)

3rd order fragmented pore bodies

- This process is recursive, till all the remainder level decomposed pore bodies of decreasing sizes that are stacked.

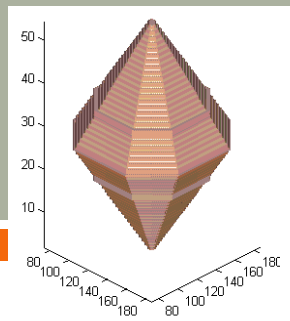

(a)(i)

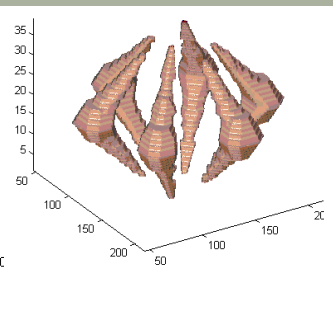

(a)(ii)

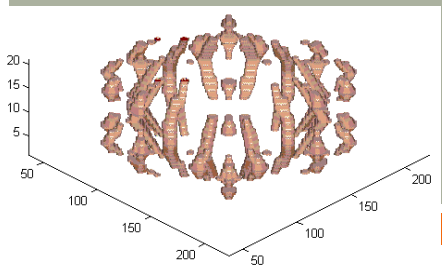

(a)(iii)

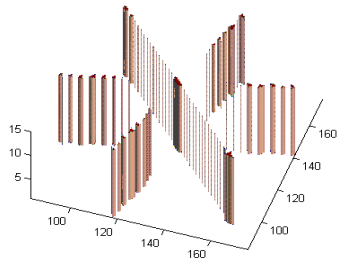

(b)(i)

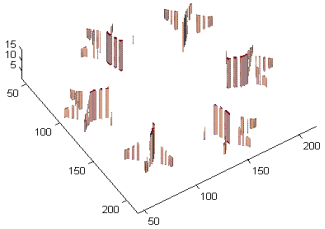

(b)(ii)

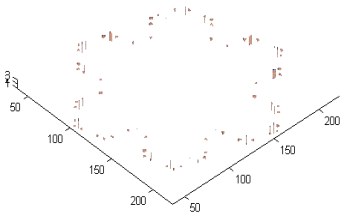

(b)(iii)

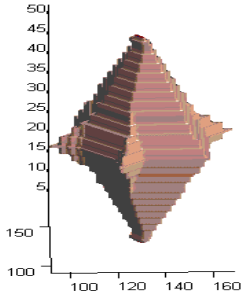

(c)(i)

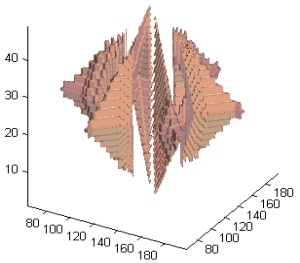

(c)(ii)

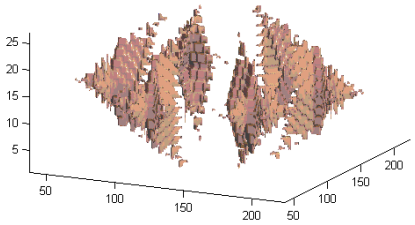

(c)(iii)

Figure 21: The diagram show the isolated of 3D reconstructed (Figure 20) from order-wise at (i) inner, (ii) middle and (iii) outer layers of

(a) pore bodies,

(b) pore channels, and

(c) pore throats.

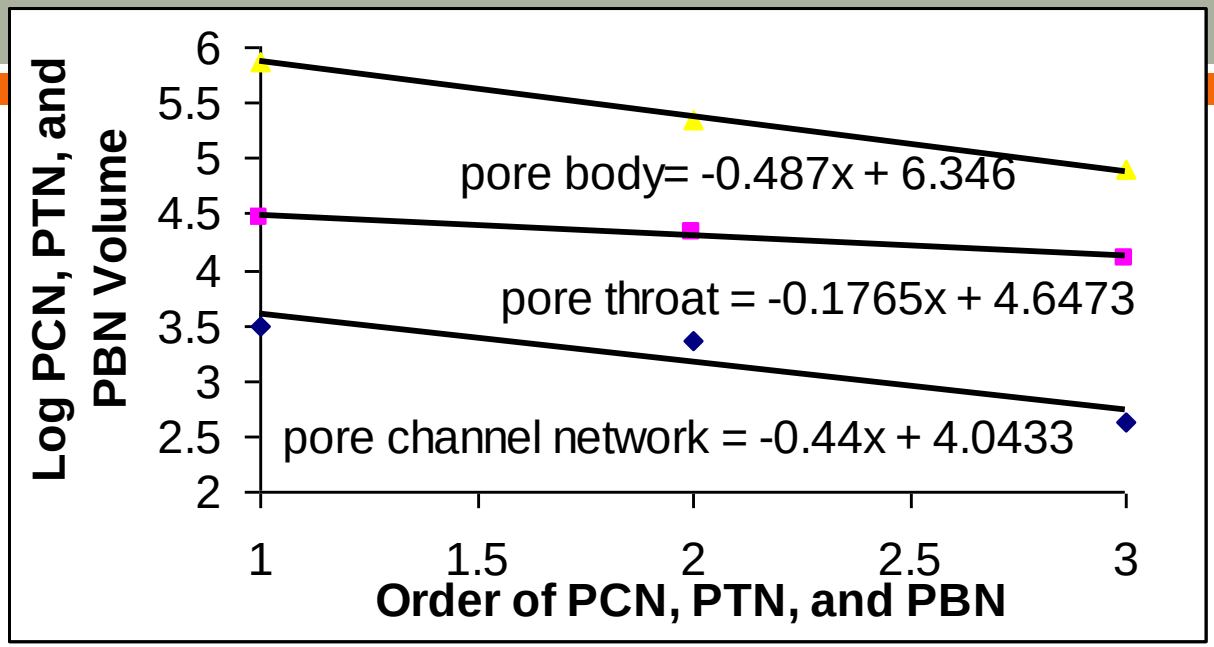

Figure 22: Distribution of order-wise of pore-channel, -throat, and –body of fractal pore.

Summary of this approach

- This ordering fragmentation approach is useful for analyzing and understanding from isolating order-wise fragmented pore channels, throats and bodies with appropriate connectivity across slices
- It is shown that the numbers of fragmented objects is increased as increasing the orders of decomposed objects
- However, the volume of respective order-wise is deceased as increasing the numbers of order.
- This entire approach can be extended to any 3D pore image (i.e., schist images) that is constructed by stacking the 2D cross sectional images.

Part II: 3D Reconstruction of schist images

- We performing CT scan imaging in order to obtain the 2D cross sectional schist images
- We consider the same methodology (i.e., pore bodies, pore channel and pore throat) performed at 3D modeling of triadic Koch curve image in constructing 3D schist rock sample
- To analyze the morphology 3D reconstruction schist rock sample, the employed structuring elements to carry out this analysis is the rhombus, square and octagon.

(a) (b)

Figure 23: (a) The photograph of schist rock sample; (b) the CT scans applied at schist rock sample

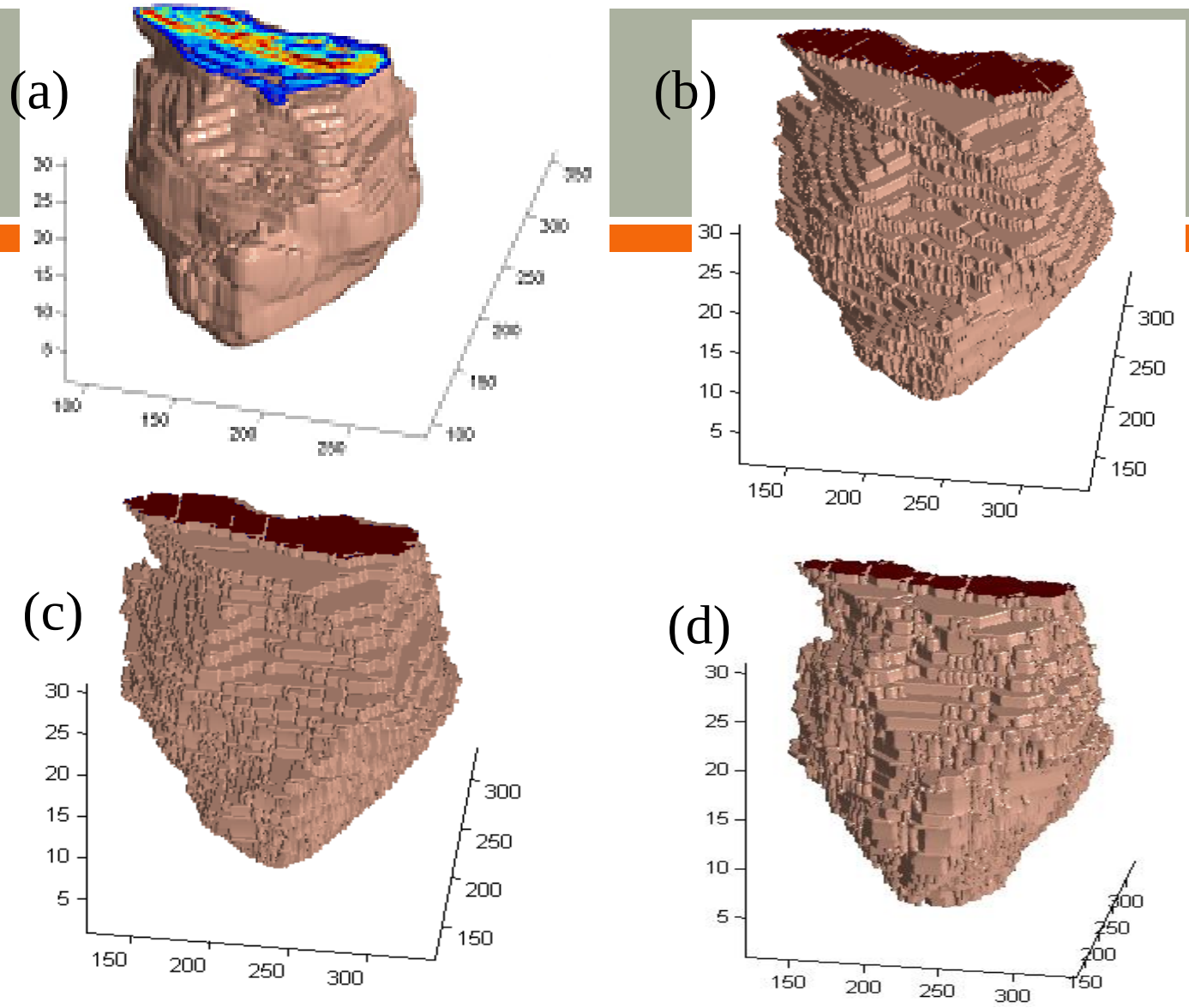

Figure 24: The 3D reconstruction of (a) binary schist image; non-overlapping decomposition technique by structuring elements of (b) rhombus, (c) square and (d) octagon

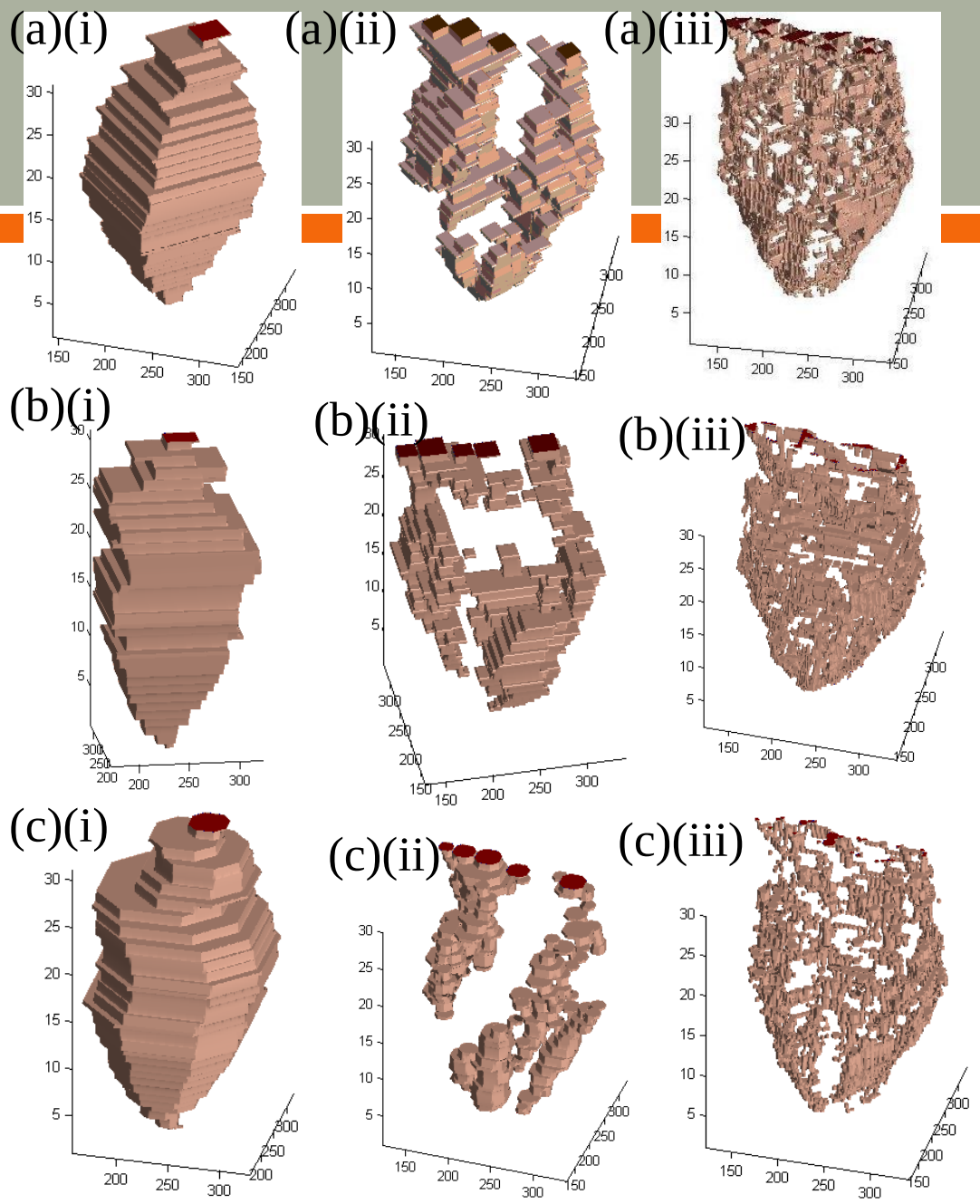

Figure 25: The diagram show the isolated 3D reconstruction image (Figure 23) from order-wise at (i) inner, (ii) middle and (iii) outer layers of pore bodies by structuring elements of

(a) rhombus

(b) square, and

(c) octagon.

Conclusions

- The algorithms employed and/or developed in this work include
  - recursive binary morphological/ opening with different shapes of structuring elements
  - Morphological skeletonization to decompose binary pore into pore-channel subsetry to reconstruct its pore phase in overlapping ways
  - Pore throat decomposition algorithm is developed and implemented
  - pore-body based order designation for pore-body, -channel, and -throat
  - proposed a set of equations to fragment the pore-body, -channel, and -throat according to regrouped orders
  - proposed a simple way to generate/ simulate flow velocity fields and their stagnant zone via morphological approaches - this approach is analogous to simulation process achieved lattice-gas automation model (LGA). This can be linked to study the intrinsic permeabilities

Thank You

Q & A